JOURNAL OF VIROLOGY, Feb. 1995, p. 809–813
0022-538X/95/$04.00+0

Vol. 69, No. 2

Identification of the Murine Coronavirus p28 Cleavage Site

SCOTT A. HUGHES, PEDRO J. BONILLA, AND SUSAN R. WEISS*

Department of Microbiology, University of Pennsylvania School of Medicine, Philadelphia, Pennsylvania 94104-6076

Received 14 September 1994/Accepted 11 November 1994

Mouse hepatitis virus strain A59 encodes a papain-like cysteine proteinase (PLP-1) that, during translation of ORF1a, cleaves p28 from the amino terminus of the growing polypeptide chain. In order to determine the amino acid sequences surrounding the p28 cleavage site, the first 4.6 kb of murine hepatitis virus strain A59 ORF1a was expressed in a cell-free transcription-translation system. Amino-terminal radiosequencing of the resulting downstream cleavage product demonstrated that cleavage occurs between Gly-247 and Val-248. Site-directed mutagenesis of amino acids surrounding the p28 cleavage site revealed that substitutions of Arg-246 (P2) and Gly-247 (P1) nearly eliminated cleavage of p28. Single-amino-acid substitutions of other residues between P7 and P2′ were generally permissive for cleavage, although a few changes did greatly reduce proteolysis. The relationship between the p28 cleavage site and other viral and cellular papain proteinase cleavage sites is discussed.

Murine coronavirus, mouse hepatitis virus strain A59 (MHV-A59), is an enveloped, positive-stranded RNA virus. Upon infection, MHV-A59 gene 1 is translated, presumably into the proteins necessary for viral RNA replication. The 31-kb viral genomic RNA is replicated, and a 3′ coterminal nested set of six subgenomic RNAs is then synthesized by the RNA-dependent RNA polymerase.

Two overlapping open reading frames (ORF1a and ORF1b) constitute gene 1 and could potentially encode an approximately 800-kDa polyprotein. It is presumed that translation of gene 1 is initiated at the 5′ end of ORF1a and either is terminated at the 3′ end of ORF1a or is continued through ORF1b via a translational frameshift near the end of ORF1a (6). Sequence analysis of gene 1 predicts ORF1b to encode the RNA polymerase and several other functional domains conserved among coronaviruses, including a helicase and zinc-finger-like motif (4, 6, 19). ORF1a is predicted to encode two papain-like proteinases and a poliovirus 3C-like proteinase (4, 19). It is thought that the ORF1a-encoded proteinases are responsible for processing both ORF1a- and ORF1b-encoded polypeptides into mature replicase proteins. The virus-encoded polymerase and proteinases are potentially important targets for antiviral therapies in that they are specific for virus replication; inhibition of these activities should not affect the host cell functions. Thus, the understanding of the structure and functions of these domains is important for the design of antiviral strategies. We have recently focused on the function of the 5′-ORF1a-encoded papain-like proteinase (PLP-1), and in this study we have begun to characterize its role in the processing of ORF1a proteins.

Polypeptides encoded in ORF1a have been detected in infected cells by using antibodies directed against sequences encoded in ORF1a. These intracellular viral proteins include the amino-terminal p28 polypeptide, p65, and a precursor polypeptide of 290 kDa which is processed into p50 and p240 (12, 16, 27). During in vitro translation of genome RNA or of synthetic RNAs derived from constructs containing amino-terminal portions of ORF1a, only p28 and a larger downstream cleavage product are detected (1, 11).

Of the predicted ORF1a-encoded proteinases, only PLP-1 has been shown to have proteolytic activity. Encoded in the first 3.43 to 4.23 kb of ORF1a, PLP-1 is responsible for *cis* cleavage of p28 during in vitro translation (1, 5). While the catalytic cysteine and histidine residues of PLP-1 have been identified for both A59 and JHM (3, 5), the p28 cleavage dipeptide is not known. Soe et al. speculated that cleavage of p28 may occur at one of two Tyr-Gly dipeptides present in the vicinity of the potential p28 cleavage region (25). However, on the basis of cleavage sites utilized by other viral papain-like proteinases (7, 9, 10, 24), it seemed more likely that cleavage would occur with a Gly or Ala in the P1 position. In the current study, we report that the p28 cleavage site occurs between Gly-247 (P1) and Val-248 (P1′). Site-directed mutagenesis identified Arg-246 (P2) and Gly-247 as critical residues for efficient cleavage.

MATERIALS AND METHODS

Construction of expression plasmid. A *Nar*I-*Hin*dIII fragment from cDNA ZA11 (20) was cloned into the *Eco*RV and *Hin*dIII sites of pSP72 (Promega), resulting in pSPZA11NH. This plasmid has MHV-A59 ORF1a sequences downstream of the bacteriophage T7 promoter. A synthetic linker containing a *Kpn*I restriction site was inserted into the *Nde*I site of this vector, downstream of the viral sequences, to create pSPZA11NHK. pSPNK was constructed by cloning a 2.89-kb *Xho*I-*Kpn*I fragment from PCR clone X1K1 (4) into the corresponding sites of pSPZA11NHK. pSPNK includes ORF1a sequences from nucleotides 182 to 4664.

PCR mutagenesis. Site-directed mutagenesis of residues Lys-241 to Lys-249 in plasmid pSPNK was accomplished by PCR (15). To decrease the probability of sequencing mistakes due to nucleotide misincorporation during amplification, Vent DNA polymerase was used (18). Specific mutations were introduced into a *Bam*HI-*Eco*RI fragment by using two complementary "inside" primers containing mismatches to the same nucleotide position of the target sequence. Recombinant PCR products were generated by using inside primers in conjunction with the corresponding upstream (Fp425-444) or downstream (Rp1347-1328) outside primers. The amplified DNA was digested with *Bam*HI and *Eco*RI and inserted into pSPNK at the same sites (Fig. 1). Arg-246→Phe was generated by inserting a specific mutation into an *Afl*II-*Eco*RI fragment as described above. Specific mutations were identified by the Sanger dideoxy sequencing method (21).

In vitro transcription-translation. In vitro transcriptions and translations were performed as described in Promega Technical Bulletin 126 by using a coupled transcription-translation rabbit reticulocyte system. Briefly, 250 ng of plasmid DNA was added per 25-μl reaction mix, which included 1,000 μCi of [^{35}S]methionine per ml. Reaction mixtures were incubated for 90 min at 30°C. Equal counts per minute of samples were added to 2× Laemmli buffer, and mixtures were incubated for 5 min at 100°C before being electrophoresed on gradient

* Corresponding author. Mailing address: Department of Microbiology, 319 Johnson Pavilion, University of Pennsylvania School of Medicine, Philadelphia, PA 19104-6076. Phone: (215) 898-8013. Fax: (215) 898-9557. Electronic mail address: weiss@mscf.med.upenn.edu.

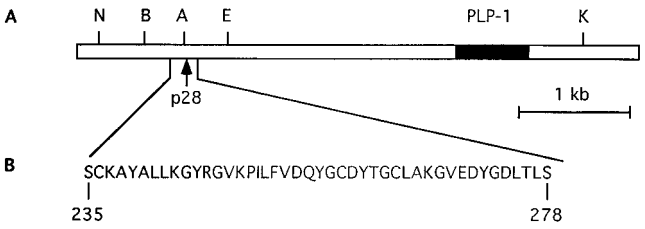

FIG. 1. Diagram of 5′ end of MHV-A59 genome and amino acid sequence surrounding predicted p28 cleavage site. (A) The 5′ region of MHV-A59 gene 1 from the *Nar*I site to the *Kpn*I restriction site was placed under the control of a T7 polymerase promoter. pSPNK encodes a 164-kDa protein that is cleaved into 28- and 136-kDa polypeptides. Restriction sites *Bam*HI, *Afl*II, and *Eco*RI were utilized during PCR mutagenesis. The predicted p28 cleavage region is indicated by an arrow, and the PLP-1 domain is depicted as a shaded region. Abbreviations: N, *Nar*I; B, *Bam*HI; A, *Afl*II; E, *Eco*RI; K, *Kpn*I; PLP-1, papain-like proteinase 1. (B) Amino acid sequence from Ser-235 to Ser-278 at and around the predicted p28 cleavage site.

	P5	P4	P3	P2	P1	P1'	P2'
TEV HC-PRO	T	Y	N	V	G	G	M
CHESTNUT BLIGHT HAV p48	D	I	L	V	G	G	Y
EQUINE ARTERITIS VIRUS nsP1	A	G	N	Y	G	G	Y
SINDBIS VIRUS nsP2 (nsP1-nsP2)	A	D	I	G	A	A	L
(nsP2-nsP3)	D	G	V	G	A	A	P
(nsP3-nsP4)	T	G	V	G	G	Y	I

FIG. 2. Cleavage sites of viral papain-like proteinases. The arrow indicates the cleavage site. TEV, tobacco etch virus; HAV, hypovirulence-associated virus.

polyacrylamide-sodium dodecyl sulfate (SDS) gels. The gels shown in Fig. 4 and 5 were processed for fluorography in Autofluor (National Diagnostic) and exposed to X-ray film.

pSPNK encodes a 164-kDa polypeptide (p164) that is processed into a 136-kDa polypeptide (p136) and a 28-kDa polypeptide (p28). Processing of p164 is inhibited by the thiol protease inhibitor leupeptin (11). In addition to producing p164, p136, and p28, transcription and translation of pSPNK produce other polypeptides that are insensitive to proteinase inhibitors and mutations of PLP-1 (3, 5, 11). These polypeptides probably represent premature termination products. The ratio of p136/(p164+p136) was used to determine the p28 cleavage efficiency of each construct. The ratio determined for the wild-type construct was designated 100% efficient, and the ratio obtained for each mutant was compared with the wild-type ratio. The ratio of cleavage product to precursor provides an internal control for the amount of protein produced in each reaction. This ratio is a more accurate reflection of cleavage efficiency than is the value obtained by measuring the absolute levels of p28, which can vary from reaction to reaction. We did not use the levels of p28 to determine the ratio of cleavage product to precursor because the counts per minute for p28 of some of the mutants were below the level of detection of the Phosphorimager. To determine the percent cleavage, levels of p164 polyprotein precursor and p136 cleavage product in nonfluorographed gels were quantitated with a Molecular Dynamics Phosphorimager.

Radiosequencing N terminus of p136. For the radiosequencing of p136, in vitro transcription and translation of pSPNK were performed as described above with either 1,000 μCi of [^{35}S]cysteine (ICN) per ml or 800 μCi of [^{3}H]leucine (ICN) per ml. Translation products were resolved by electrophoresis on 5 to 12% polyacrylamide–SDS gradient gels. Electrophoretic transfer onto a polyvinylidene difluoride membrane (Bio-Rad) was performed at 1.0 A for 3 h in 0.5× Towbin buffer (26). After exposure of dried membrane to X-ray film, the p136 cleavage product was located and excised by using the autoradiogram as a key. Edman degradation was performed on 100 mm^2 of membrane to which p136 was immobilized. The eluate from each cycle was collected, added to scintillation cocktail (ICN), and counted in a liquid scintillation counter.

RESULTS

Identification of the p28 cleavage site. In order to determine the amino acid sequence surrounding the p28 cleavage site, we used the polypeptides synthesized during transcription-translation of the pSPNK construct. This construct contains ORF1a sequence downstream of the T7 RNA bacteriophage polymerase promoter from nucleotides 182 to 4664, which includes the region encoding p28 through PLP-1. During transcription and translation of this plasmid, a large polypeptide of 164 kDa is synthesized and quickly processed into p28 and the downstream product, p136 (2, 11). This system provides a simple assay for p28 cleavage. Sequencing of the amino terminus of p136 would provide the sequences at the in vitro cleavage site of p28. Because expression in reticulocyte lysates does not produce enough protein for microsequencing and our attempts at expressing this plasmid in *Escherichia coli* to obtain higher levels of protein were unsuccessful, we turned to sequencing of radiolabeled p136 synthesized in the coupled transcription-translation reticulocyte system. From the electrophoretic mobility of p28, we predicted that cleavage of p28 occurs somewhere between Ser-235 and Gly-258. On the basis of cleavage sites utilized by other viral papain-like proteinases (Fig. 2), we focused on sites with Gly or Ala in the P1 position. We then determined that mapping Cys and Leu residues near the amino terminus of p136 would allow us to unambiguously determine the cleavage site.

Thus, to determine the amino terminus of the downstream cleavage product, sequencing of both [^{3}H]Leu- and [^{35}S]Cys-labeled p136 was carried out (Fig. 3). After 10 cycles of Edman degradation of [^{3}H]Leu-labeled p136, a peak was observed in cycle 5 (Fig. 3). The radioactivity observed in fraction 1 is an artifact caused by nonspecific radioactive material which elutes in the first cycle (25a). After 20 cycles of Edman degradation of [^{35}S]Cys-labeled p136, peaks were observed in fractions 12 and 17 (Fig. 3). The radioactivity observed in fraction 18 is a result of carryover from previous cycles. This is a phenomenon that occurs because of the inefficient nature of amino acid cleavage

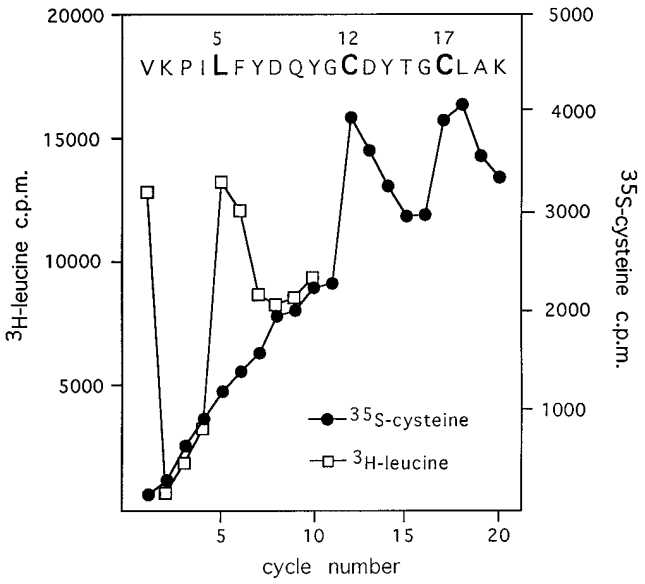

FIG. 3. N-terminal radiosequence analysis of p136. The downstream 136-kDa cleavage product was generated by coupled in vitro transcription and translation of pSPNK in the presence of either [^{35}S]cysteine or [^{3}H]leucine. Radiolabeled p136 was analyzed by Edman degradation, and the radioactivity in the resulting fraction was determined. The deduced amino-terminal amino acid sequence of p136 is shown by single-letter amino acid code, with cysteine and leucine residues in boldface. Cycle numbers are shown above leucine and cysteine residues.

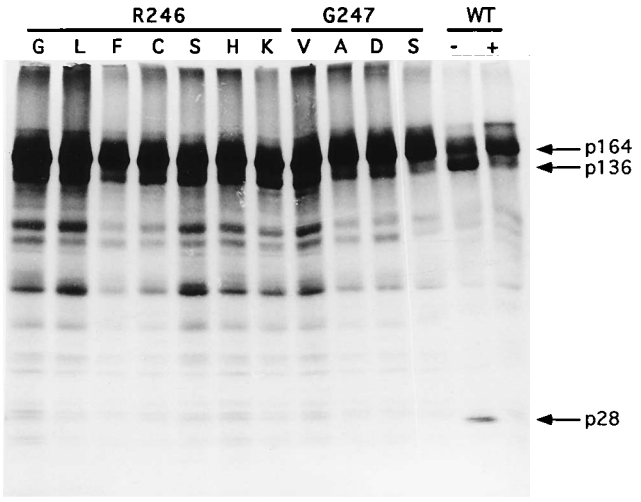

FIG. 4. In vitro translation and processing of pSPNK polyproteins containing mutagenized Arg-246 or Gly-247 residues. Polyproteins were synthesized and analyzed as described in Materials and Methods. Wild-type transcripts of pSPNK encode a 164-kDa polyprotein that is processed into 28- and 136-kDa polypeptides. The migratory positions of p164, p136, and p28 are indicated by arrows. The wild-type residues are shown at the top, and the amino acid substitutions are indicated above each lane. Synthesis and processing of wild-type polyprotein were carried out in the absence (−) or presence (+) of 2 mM leupeptin. The single-letter amino acid code is used. Abbreviation: WT, wild type.

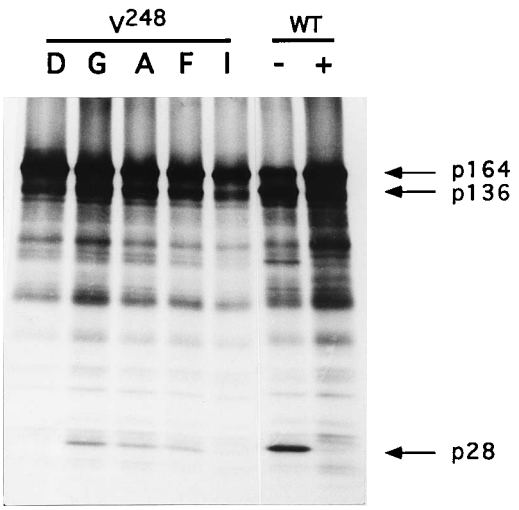

FIG. 5. In vitro translation and processing of pSPNK polyproteins containing mutagenized Val-248 residues. Polyproteins were synthesized and analyzed as described in Materials and Methods. Mutations, positions of polypeptides, and abbreviations are indicated as in Fig. 4.

during Edman degradation. With each successive cycle of Edman degradation, this carryover effect becomes more significant (25a). The profile obtained was $(aa)_4$ Leu $(aa)_6$ Cys $(aa)_4$ Cys. This pattern fits with the known amino acid sequence of MHV-A59 ORF1a (4), in which there is Leu at residue 253 and Cys at residues 259 and 264. The above data are consistent only with cleavage occurring between Gly-247 and Val-248. These data are not consistent with cleavage at any other sites in the region encoded by the plasmid pSPNK, which includes the first 4.6 kb of the genome.

Characterization of the p28 cleavage site. Identification of Gly-247 and Val-248 as the dipeptide cleaved by PLP-1 allows for further definition of amino acids required for efficient cleavage of p28. Eight sets of mutations from the P7 position to the P2′ position were introduced into the pSPNK construct, and the effect on cleavage was assayed by using the rabbit reticulocyte coupled transcription-translation system as described above. The gels in Fig. 4 and 5 show the effect of mutagenesis of the amino acids in the P2 (Arg-246), P1 (Gly-247), and P1′ (Val-248) positions on cleavage of p28. To quantitate the inhibition of cleavage as a result of mutagenesis, we carried out assays using constructs with mutations in amino acids 241 through 249. The efficiency of cleavage for each mutant was determined as described in Materials and Methods (Fig. 6). The gels from which Fig. 6 was derived are not shown (see Materials and Methods). Both conservative and nonconservative changes of Gly-247 in the P1 position reduced cleavage by over 80% in comparison with the wild-type levels (Fig. 4 and 6). These levels of inhibition are consistent with the microsequencing analysis which identified Gly-247 as the P1 residue. Furthermore, these data show that cleavage with MHV PLP-1 is similar to cleavages carried out by other viral papain-like proteinases which require small uncharged amino acids in the P1 position for efficient cleavage (8, 10, 22–24). Substitution of Arg-246 in the P2 position also resulted in dramatic inhibition of p28 cleavage (Fig. 4 and 6). Substitution of Arg-246 for His or Lys also inhibited cleavage, indicating that positive charge alone in the P2 position is not sufficient for cleavage of p28. Substitution of either Gly-247 or Arg-248 resulted in levels of inhibition greater than or equal to that caused by the addition of the thiol protease inhibitor leupeptin, which previously has been shown to be a potent inhibitor of p28 cleavage (11). Substitutions of Val in the P1′ position with either Gly or Ala did not significantly reduce cleavage, although other less conservative substitutions such Asp or Ile did inhibit cleavage by over 60% (Fig. 5 and 6). This suggests that there are some requirements for the P1′ position.

Amino acid substitutions at the P7, P5, P3, and P2′ positions were tolerated (Fig. 6). Although cleavage was reduced somewhat in most cases, substitution of these residues did not affect cleavage to the degree seen with mutagenesis of either the P2 or P1 position. For example, substitution of the aromatic Tyr-245 in the P3 position with a closely related Phe residue did not

P7	P6	P5	P4	P3	P2	P1	P1'	P2'
Leu241	**Leu242**	**Lys243**	**Gly244**	**Tyr245**	**Arg246**	**Gly247**	**Val248**	**Lys249**
Pro +	N.D.	Thr +	Val +/-	Cys +	Cys -	Val -	Asp -	Arg +
Arg +			Ala +	Ser +	Ser -	Ala -	Ala +	Met +
His +/-			Asp +	Phe ++	Gly-	Asp -	Gly ++	Thr +/-
					Leu -	Ser-	Phe+	
					His-	Cys-	Ile +/-	
					Lys -			
					Phe-			

FIG. 6. Wild-type amino acid sequence and substitutions around the p28 cleavage site. The wild-type amino acid sequence from the P7 position to the P2′ position is indicated in boldface. Corresponding substitutions are shown directly below the wild-type residues. The notations −, +/−, +, and ++ indicate >80% inhibition, 60 to 80% inhibition, 40 to 60% inhibition, and 20 to 40% inhibition, respectively. Mutations were introduced as described in Materials and Methods. Quantitation of percent inhibition of cleavage relative to the wild-type level was carried out as described in Materials and Methods. Gels used to quantitate percent inhibition are not shown. The scissile bond is between the P1 and P1′ residues.

significantly affect cleavage. This is in sharp contrast to the outcome with conservative substitutions, which have dramatic effects in the P1 and P2 positions.

DISCUSSION

In this report, we have demonstrated that p28 cleavage occurs between Gly-247 and Val-248. This is the first identification of a cleavage site in the large polypeptide encoded in the 21-kb replicase gene (gene 1) of MHV and the first cleavage site identified for any coronavirus proteinase. It has been shown previously that this cleavage is carried out by PLP-1 encoded in ORF1a. Further characterization of the amino acids surrounding the cleavage site demonstrates that Arg-246 and Gly-247 in the P2 and P1 positions, respectively, are required for cleavage of p28. Val-248 in the P1′ position and residues in positions P7, P6, P5, P4, P3, and P2′ were not essential for cleavage, although most substitutions did result in some inhibition of cleavage. Substitution of Tyr-245 in the P3 position with Phe did not affect cleavage, suggesting the necessity for an aromatic ring in the P3 position, rather than Tyr itself, for efficient cleavage.

Sequence alignment analysis of MHV-A59, MHV-JHM, and human coronavirus 229E reveals that the RG dipeptide is conserved in all three strains. In 229E, the P1′ Val, which is conserved in MHV-A59 and MHV-JHM, is replaced with a Gly residue (14). In MHV-A59, Val-248→Gly permits efficient cleavage of p28, indicating that the cleavage site has been relatively conserved among these mouse and human coronavirus strains. Cleavage at the GG dipeptide in ORF1a of 229E would generate an approximately 12-kDa polypeptide (14).

On the basis of sequence analysis, PLP-1 of MHV-A59 appears to belong to a family of viral papain-like cysteine proteinases (13); this family contains both animal and plant viral proteinases, including the potyviral HC proteinase, Sindbis virus nsP2, and the papain-like proteinases encoded by chestnut blight hypovirulence-associated virus and equine arteritis virus (13, 24). The cleavage sites of these proteinases, which include tobacco etch virus HC-Pro (7, 8), chestnut blight hypovirulence-associated virus p48 (9, 22), equine arteritis virus nsP1 (24), and Sindbis virus nsP2 (10, 23), have been determined and characterized and are listed in Fig. 2. All of these proteinases cleave at sites which have Gly or Ala, uncharged residues with short side chains, in the P1 position. It is therefore not surprising to see that PLP-1 of MHV also requires a Gly in the P1 position.

On the basis of a sequence alignment of the rubella virus proteinase and cellular papain-like proteinases, it was originally suggested by Gorbalenya et al. that this group of viral cysteine proteinases resembles the papain-like cellular proteinases (13). While the cellular and viral proteinases share conserved Cys and His catalytic residues at similar distances within the proteinase domains, as well as an aromatic amino acid following the catalytic Cys residue, there is little other sequence homology between the cellular and viral proteinases. Our results suggest that Arg-246 in the P2 position is a critical residue required for cleavage by MHV PLP-1. Interestingly, the P2 position is a critical residue for cleavage by papain and some of the related cellular proteinases (17). This group of cellular enzymes usually prefers Phe in the P2 position. However, the same proteinases can utilize, to different extents, substrates in which the Phe in the P2 position is replaced with Arg. Those proteinases that can utilize Arg have a conserved glutamic acid residue in the substrate-binding pocket which is thought to allow the positioning of the Arg residue in the substrate (17). The question of whether the coronavirus papain-like proteinases also contain a conserved negatively charged amino acid in the substrate-binding pocket remains to be answered. The structure of PLP-1 remains to be elucidated. Understanding the structure of the viral proteinases may be important in the design of antiviral strategies.

ACKNOWLEDGMENTS

This work was supported by NIH grants AI-17418 and NS-21954. S.A.H. and P.J.B. were partially supported by NIH training grant NS01780.

We thank Xiurong Wang for excellent technical assistance; Mikhail Rozanov for many discussions and helpful suggestions; and the Wistar protein core facility, directed by David Speicher, for carrying out the protein microsequencing.

REFERENCES

1. **Baker, S. C., N. LaMonica, C. K. Shieh, and M. M. C. Lai.** 1990. Murine coronavirus gene 1 polyprotein contains an autocatalytic activity. Adv. Exp. Med. Biol. **276:**283–290.
2. **Baker, S. C., C. K. Shieh, M. F. Chang, D. M. Vannier, and M. M. C. Lai.** 1989. Identification of a domain required for autoproteolytic cleavage of murine coronavirus gene A polyprotein. J. Virol. **63:**3693–3699.
3. **Baker, S. C., K. Yokomori, S. Dong, R. Carlisle, A. E. Gorbalenya, E. V. Koonin, and M. M. C. Lai.** 1993. Identification of the catalytic sites of a papain-like proteinase of murine coronavirus. J. Virol. **67:**6056–6063.
4. **Bonilla, P. J., A. E. Gorbalenya, and S. R. Weiss.** 1994. Mouse hepatitis virus strain A59 RNA polymerase gene ORF 1a: heterogeneity among MHV strains. Virology **198:**736–740.
5. **Bonilla, P. J., J. L. Piñón, S. A. Hughes, and S. R. Weiss.** Characterization of the leader papain-like protease of MHV-A59. Adv. Exp. Med. Biol., in press.
6. **Bredenbeek, P. J., C. J. Pachuk, A. F. H. Noten, J. Charite, W. Luytjes, S. R. Weiss, and W. J. M. Spaan.** 1990. The primary structure and expression of the second open reading frame of the polymerase gene of the coronavirus MHV-A59; a highly conserved polymerase is expressed by an efficient ribosomal frameshifting mechanism. Nucleic Acids Res. **18:**1825–1832.
7. **Carrington, J. C., S. M. Cary, T. D. Parks, and W. G. Dougherty.** 1989. A second proteinase encoded by a plant potyviral genome. EMBO J. **8:**365–370.
8. **Carrington, J. C., and K. L. Herndon.** 1992. Characterization of the potyviral HC-Pro autoproteolytic cleavage site. Virology **187:**308–315.
9. **Choi, G. H., R. Shapira, and D. L. Nuss.** 1991. Cotranslational autoproteolysis involved in gene expression from a double stranded RNA genetic element associated with hypovirulence of the chestnut blight fungus. Proc. Natl. Acad. Sci. USA **88:**1167–1171.
10. **DeGroot, R., W. R. Hardy, Y. Shirako, and J. H. Strauss.** 1990. Cleavage site preferences of Sindbis virus polyproteins containing the non-structural proteinase. Evidence for temporal regulation of polyprotein processing *in vivo*. EMBO J. **9:**2631–2638.
11. **Denison, M. R., and S. Perlman.** 1986. Translation and processing of mouse hepatitis virus virion RNA in a cell-free system. J. Virol. **60:**12–18.
12. **Denison, M. R., P. W. Zoltick, S. A. Hughes, B. Giangreco, A. L. Olson, S. Perlman, J. L. Leibowitz, and S. R. Weiss.** 1992. Intracellular processing of the N-terminal ORF 1a proteins of the coronavirus MHV-A59 requires multiple proteolytic events. Virology **189:**274–284.
13. **Gorbalenya, A. E., E. V. Koonin, and M. M. C. Lai.** 1991. Putative papain-related thiol proteases of positive strand RNA viruses. FEBS Lett. **288:**201–205.
14. **Herold, J., T. Raabe, B. Schelle-Prinz, and S. G. Siddell.** 1993. Nucleotide sequence of the human coronavirus 229E RNA polymerase locus. Virology **195:**680–691.
15. **Higuchi, R., B. Krummel, and R. K. Saiki.** 1988. A general method of *in vitro* preparation and specific mutagenesis of DNA fragments: study of protein and DNA interactions. Nucleic Acids Res. **16:**7351–7367.
16. **Hughes, S. A., M. L. Dension, P. J. Bonilla, J. L. Leibowitz, and S. R. Weiss.** 1993. A newly identified MHV-A59 ORF 1a polypeptide p65 is temperature sensitive in two RNA negative mutants. Adv. Exp. Med. Biol. **342:**221–226.
17. **Khouri, H. E., T. Vernet, R. Menard, F. Parlatti, P. Laflamme, D. C. Tessier, B. Gour-Salin, D. Y. Thomas, and A. C. Storer.** 1991. Engineering of papain: selective alterations of substrate specificity by site-directed mutagenesis. Biochemistry **30:**3929–3936.
18. **Kong, H., R. B. Kucera, and W. E. Jack.** 1993. Characterization of a DNA polymerase from the hyperthermophile archaea *Thermococcus litoralis*. Vent polymerase, steady state kinetics, thermal stability, processivity, strand displacement and exonuclease activities. J. Biol. Chem. **268:**1965–1975.
19. **Lee, H. J., C. K. Shieh, A. E. Gorbalenya, E. V. Koonin, N. LaMonica, J. Tuler, A. Bagdzhadzhyan, and M. M. C. Lai.** 1991. The complete sequence

of the murine coronavirus gene 1 encoding the putative protease and RNA polymerase. Virology **180:**567–582.
20. **Pachuk, C. J., P. J. Bredenbeek, P. W. Zoltick, W. J. M. Spaan, and S. R. Weiss.** 1989. Molecular cloning of the gene encoding the putative polymerase of mouse hepatitis virus strain A59. Virology **171:**141–148.
21. **Sanger, F., S. Nicklen, and A. R. Coulson.** 1977. DNA sequencing with chain-terminating inhibitors. Proc. Natl. Acad. Sci. USA **74:**5463–5467.
22. **Shapira, R., and D. L. Nuss.** 1991. Gene expression by a hypovirulence-associated virus of the chestnut blight fungus involves two papain-like protease activities. J. Biol. Chem. **266:**19419–19425.
23. **Shirako, Y., and J. H. Strauss.** 1990. Cleavage between nsP1 and nsP2 initiates the processing pathway of Sindbis virus nonstructural polyprotein P123. Virology **177:**54–64.
24. **Snijder, E. J., A. L. M. Wassenaar, and W. J. M. Spaan.** 1992. The 5′ end of the equine arteritis virus replicase gene encodes a papainlike cysteine protease. J. Virol. **66:**7040–7048.
25. **Soe, L. H., C.-K. Shieh, S. C. Baker, M.-F. Chang, and M. M. C. Lai.** 1987. Sequence and translation of the murine coronavirus 5′-end genomic RNA reveals the N-terminal structure of the putative RNA polymerase. J. Virol. **61:**3968–3976.
25a. **Speicher, D.** Personal communication.
26. **Towbin, H., T. Staehelin, and J. Gordon.** 1979. Electrophoretic transfer of proteins from polyacrylamide gels to nitrocellulose sheets: procedure and some applications. Proc. Natl. Acad. Sci. USA **76:**4350–4354.
27. **Weiss, S. R., S. A. Hughes, P. J. Bonilla, J. L. Leibowitz, and M. L. Denison.** 1994. Coronavirus polyprotein processing. Arch. Virol. **9**(Suppl.)**:**349–358.